Spectrochimica Acta Part A: Molecular and Biomolecular Spectroscopy 98 (2012) 170–177

Contents lists available at SciVerse ScienceDirect

Spectrochimica Acta Part A: Molecular and Biomolecular Spectroscopy

journal homepage: www.elsevier.com/locate/saa

Synthesis, luminescence properties of Eu(III) and Tb(III) complexes with a novel aromatic carboxylic acid and their interactions with bovine serum albumin

Liqun Shen [a], Zhengfa Yang [b], Ruiren Tang [b,*]

[a] College of Chemistry and Chemical Engineering, Guangxi University for Nationalities, Guangxi Key Laboratory of Chemistry and Engineering of Forest Products, Nanning 530006, PR China
[b] School of Chemistry and Chemical Engineering, Central South University, Changsha 410083, PR China

HIGHLIGHTS

- A novel ligand and its Eu(III) and Tb(III) complexes were synthesized.
- The luminescence properties of Eu(III) and Tb(III) complexes were studied.
- The binding characteristics of **L**, Eu**L** and Tb**L** with BSA were investigated.
- UV–Vis and synchronous fluorescence indicated the changed conformation of BSA.
- The binding affinity with BSA was determined to be in the order of Tb**L** > Eu**L** > **L**.

GRAPHICAL ABSTRACT

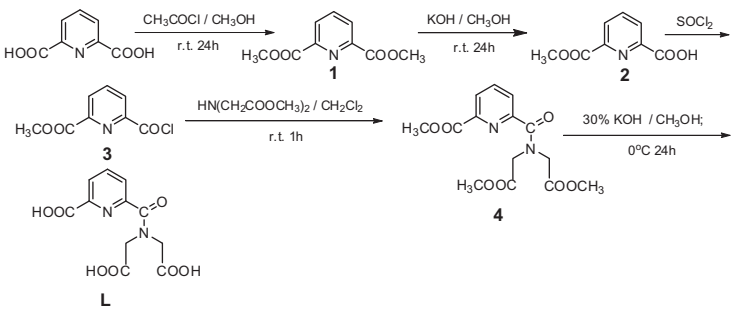

ARTICLE INFO

Article history:
Received 3 February 2012
Received in revised form 11 August 2012
Accepted 20 August 2012
Available online 27 August 2012

Keywords:
Synthesis
Dimethyl pyridine-2,6-dicarboxylate
Coordination
Lanthanide complex
Luminescence
Bovine serum albumin

ABSTRACT

A novel aromatic carboxylic acid ligand (**L**) was synthesized and its corresponding Eu(III) and Tb(III) complexes, $Na_3EuLCl_3{\cdot}2H_2O$ (Eu**L**) and $Na_3TbLCl_3{\cdot}3H_2O$ (Tb**L**), were successfully prepared. **L** and its corresponding complexes were characterized by means of MS, elemental analysis, IR, ^1H NMR and TG. The luminescence spectra of Eu(III) and Tb(III) complexes were investigated and the results showed that **L** was an efficient sensitizer for Eu(III) and Tb(III) luminescence. The interactions of **L**, Eu**L** and Tb**L** with bovine serum albumin (BSA) have been investigated through fluorescence spectroscopy under physiological conditions. The Stern–Volmer analysis indicated that the fluorescence quenching of BSA by **L**, Eu**L** and Tb**L** was resulted from static mechanism, and the binding constants (K_a) were 2.22×10^4, 1.33×10^5 and 4.27×10^5 at 300 K, respectively. The binding sites (n) and the corresponding thermodynamic parameters ΔH, ΔS, and ΔG were calculated at different temperatures. According to the theoretical and experimental results, van der Waals interactions and hydrogen bonds were found to play major roles in the binding reaction. Furthermore, UV–Vis absorption spectroscopy and synchronous fluorescence spectra indicated that the conformation of BSA was changed. The results obtained in the work can help understand the action mode between **L** and its corresponding Eu(III) and Tb(III) complexes with BSA, and they are also expected to provide important information of designs of new inspired drugs based on Eu and Tb.

Introduction

In recent years, the rational design and synthesis of lanthanide organic coordination complexes have received special attention for their fascinating architectures and potential application as functional materials [1]. In particular, Ln(III) complexes are more popular due to their well-defined luminescence properties, including hypersensitivity to the coordination environment, narrow bandwidth and millisecond luminescence decay times. For example, the Ln(III) complexes have been widely used in diagnostic tools, luminescence sensors, laser systems, and optical amplification for

* Corresponding author. Tel.: +86 731 88836961; fax: +86 731 88879616.
E-mail address: trr@mail.csu.edu.cn (R. Tang).

1386-1425/$ - see front matter © 2012 Elsevier B.V. All rights reserved.
http://dx.doi.org/10.1016/j.saa.2012.08.060

telecommunications [1–4]. Nevertheless, the Ln(III) complexes usually give weak luminescence due to the weak absorption coefficient of the parity-forbidden f–f transitions which limits their practical application considerably. This can be overcome by the use of high absorbent chelating ligands, which served as efficient sensitizers. Much work has been done, but the effects on the luminescence properties of rare-earth complexes still need to be further studied.

Pyridine-2,6-dicarboxylic acid (H_2DPC) possesses biological activity in the body of the animal and plant. Its derivatives and complexes were studied extensively and were used in all sorts of fields [5,6]. In the past few years, many studies on the molecular structure of metal complexes and their biological activities aroused much interest in the field of inorganic chemistry [7,8]. It was found that the rare earth metals possessed a special affinity to tumor cells. For instance, 70% of ^{169}Yb was found to accumulate in tumors 10 min after intravenous injection [9]. Also, the luminescent Eu and Tb complexes were capable of selectively binding to 'drug site II' of serum albumin and played a significant part in drug pharmacokinetics and pharmacodynamics [10]. Serum albumins are the major soluble protein constituents of the circulatory system and have many physiological functions. The most important property of this group of proteins is that they serve as transporters for a variety of compounds. Therefore, the study of the interactions between the rare earth metal complexes and serum albumins is important for the exploration of their biological effects and drug screening. BSA serves well as protein model for the study due to its structural homology with human serum albumin (HSA) [11,12]. Fluorescence spectroscopy is one of the powerful tools to explore the interaction between the small molecule and bio-macromolecule [13]. Thus, it is useful to study the interactions of the small molecules and the small molecule complexes with, taking the quenching of the intrinsic tryptophan fluorescence of BSA as a tool. The study of the interaction mechanism between drugs or the small molecules with serum albumins shows great significance in pharmacokinetics, and it has proved to be one of the most important research subjects in life science, chemistry and clinical medicine.

Mostly, many studies focused on the introducing of the coordination function groups to the H_2DPC, resulted in the sensitization of the rare earth ions [14,15]. Nevertheless, the studies on the asymmetric ligands containing pyridine-2,6-dicarboxylic acid unit, are rarely reported. In this paper, a novel asymmetrical chelating ligands containing pyridine-2,6-dicarboxylic acid unit and their complexes with Eu(III) and Tb(III) were successfully prepared. The luminescence spectra of Eu and Tb complexes have been studied and they were proved to be efficient sensitizers. Moreover, the interaction mechanism between **L**, Eu**L**, Tb**L** and BSA were investigated, which was of great importance to understand the general rules of their interactions and showed the reference value to the design of new drugs as well. The synthetic route of **L** was expressed in Scheme 1.

Experimental

Materials and methods

The stock solution of BSA (purity ⩾99%, purchased from Sino-Biotechnology Company, Shanghai, China) was prepared to be the concentration of 1.0×10^{-5} mol L^{-1} by dissolving it in 0.1 M HCl–Tirs buffer solution (pH 7.4, 50 mM NaCl), and kept it in the dark at 0–4 °C. After **L** and its Eu(III) and Tb(III) complexes were dissolved in water, and diluted to the desired concentration, the working solutions of **L**, Eu(III) and Tb(III) complexes were obtained. The buffer Tris was purchased from Acros (Geel, Belgium). Dimethyl pyridine-2,6-dicarboxylate **1** was prepared by literature [16]. Other chemicals were of A.R. grade and used without further purification. The water used in this study was doubly deionized.

Melting points were determined on a XR-4 apparatus (thermometer uncorrected). Elemental analysis was carried out by a PerkinElmer 2400 elemental analyzer. Infrared spectra (4000–400 cm^{-1}) were recorded with KBr discs as sample by a Nicolet NEXUS 670 FT-IR spectrophotometer. ^{1}H NMR was measured with a Bruker-400 MHz nuclear magnetic resonance spectrometer with $CDCl_3$, DMSO and D_2O as solvents and TMS as internal reference. The EI-mass spectra were recorded on a Finnigan MAT 90 instrument. UV–Vis spectra were carried out by TU-1800 spectrophotometer made by LabTech in Beijing, China. Excitation and Emission spectra were recorded on a Hitich F-4500 luminescence spectrophotometer (The width of emission detector slit and the voltage of photomultiplier tube were 2.5 nm and 700 V respectively for Eu(III) complex; while 5 nm and 400 V for Tb(III) complex correspondingly in solid state). Thermal gravimetric (TG) were performed in the nitrogen atmosphere using a Netzsch TG 209 thermogravimetric analyzer at a heating rate of 10 °C min^{-1} from 20 to 700 °C.

*Preparation of **L***

*Synthesis of 6-(methoxycarbonyl) pyridine-2-carboxylic acid (**2**)*

A solution of **1** (5.85 g, 30.0 mmol) in methanol (150 mL) was cooled to 0 °C. After KOH pellets (1.76 g, 31.0 mmol) were added, the reaction mixture was stirred at 0 °C for 2 h and then at room temperature for 24 h. The solvent was removed under reduced pressure, and the residue was suspended in H_2O (100 mL) and extracted with ethyl acetate (3 × 30 mL). The aqueous layers were acidified to pH 3 with 1 M diluted HCl solution and extracted with chloroform (5 × 30 mL). The collected organic layers were dried over anhydrous Na_2SO_4. The chloroform was removed in vacuo to provide the desired product **2** (2.80 g, 52%) as a white solid: m.p. 144–146 °C. ^{1}H NMR (DMSO-d_6): δ_H 8.12–8.24 (m, Py-3,4,5,3H) 3.93 (s, $-CH_3$,3H); ^{13}C NMR(DMSO-d_6): δ = 52.2, 127.4, 127.7, 139.0, 147.4, 148.9, 164.9, 165.8 ppm; IR (KBr), ν/cm^{-1}: 3073, 2964, 2852, 1725, 1581, 1325.

*Synthesis of methyl 6-(chlorocarbonyl) pyridine-2-carboxylate (**3**)*

2 (0.72 g, 4 mmol) was treated with thionyl chloride (10 mL) and one drop of *N*,*N*-dimethylformamide, then the mixture was refluxed at 70 °C for 4 h. The excess thionyl chloride was removed by evaporation under reduced pressure. Residual thionyl chloride was further removed by co-evaporation with 30 mL of anhydrous benzene to afford the corresponding acid chloride **3**. This crude product was used in the following step without further purification.

*Synthesis of methyl 6-[N,N-bis(methoxycarbonyl methyl) carbamoyl]pyridine-2-carboxylate (**4**)*

Dimethyl iminodiacetate (0.56 g, 3.5 mmol) and triethylamine (0.35 g, 3.5 mmol) were dissolved in 15 mL of dichloromethane, stirring at 0 °C, and then **3** (0.7 g, 3.5 mmol) was added in three portions with continuous stirring at 0 °C. The reaction mixture was stirred at room temperature for 1 h. After the solvent was removed under reduced pressure, the residue was dissolved in ethyl acetate and water (15:15, v:v). The aqueous phase was extracted with ethyl acetate (2 × 5 mL). Then, the organic phase was combined and dried by anhydrous Na_2SO_4. After the solvent was removed under reduced pressure, the crude was further purified by column chromatography with petroleum ether and ethyl acetate (1:1) to give **4** (0.9 g, 81.8%) as a white solid: m.p. 80–82 °C. Anal. Calcd for $C_{14}H_{16}N_2O_7$ (%): C, 51.85; H, 4.97; N, 8.64; Found: C, 51.72; H, 4.91; N, 8.62; ^{1}H NMR ($CDCl_3$): δ 8.16 (q, *J* = 7.2 Hz Py-3,5, 2H), 7.98 (t, *J* = 8.0 Hz, Py-4, 1H), 4.52 (s, N–CH_2, 2H), 4.41

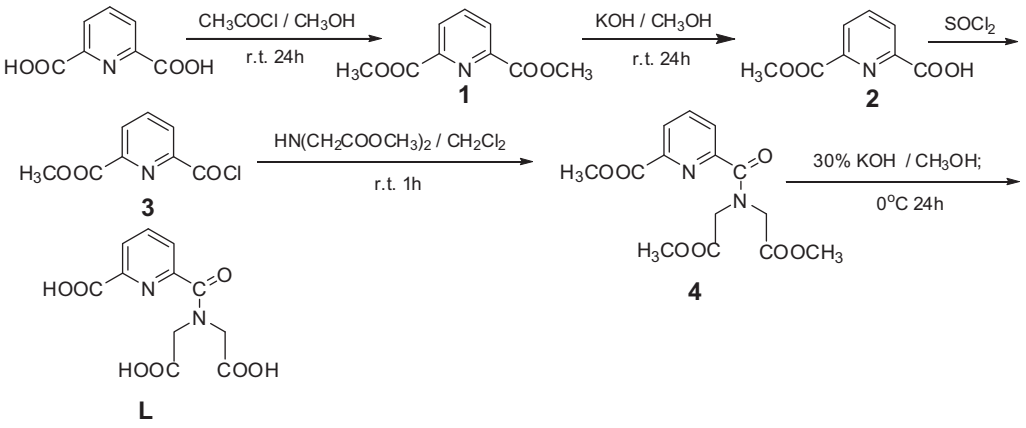

Scheme 1. The synthetic route of L.

(s, N–CH_2, 2H), 3.97 (s, Py-2-OCH_3, 3H), 3.83 (s, –CH_3, 3H), 3.79 (s, –CH_3, 3H); IR (KBr), ν/cm^{-1}: 3093, 3013, 2954, 1748, 1719, 1635, 1214, 1189; EI-MS: *m/z*: 324.3[M]$^+$.

*Synthesis of 6-[N,N-bis(ethyloic)carbamoyl]pyridine-2-carboxylic acid (**L**)*

4 (0.81 g, 2.5 mmol) was dissolved in 50 mL anhydrous methanol with stirring in an ice bath. 2.5 g KOH solution (30%) were added, and the reaction mixture was stirred at 0 °C for 24 h. Then the solvent was evaporated to give a yellow oily residue, which was purified by a 732 cation exchange resin column to provide **L** (0.68 g, 96.5%) as a white solid. m.p. 198–200 °C. Anal. Calcd for $C_{11}H_{10}N_2O_7$ (%): C, 46.82; H, 3.57; N, 9.93; Found: C, 46.91; H, 3.55; N, 9.89; ^{1}H NMR (H_2O): δ 8.11-8.23 (m, Py-3,5, 2H), 7.89 (d, *J* = 8.0 Hz, Py-4, 1H), 4.38 (s, N–CH_2, 2H),4.28 (s, N–CH_2, 2H); IR (KBr), ν/cm^{-1}: 3078, 2663, 1716, 1616, 1425, 1389, 1351; EI-MS: *m/z*: 282.2[M]$^+$.

Preparation of the complexes

A mixture of **L** (0.8 mmol) and a solution of $LnCl_3{\cdot}6H_2O$ (0.8 mmol) (Ln = Tb, Eu) in H_2O (6 mL) was stirred for 10 min at room temperature, following which the aqueous NaOH (0.01 M) was added dropwise to pH 6.0. Then the mixture was stirred at 60 °C for 12 h. The resulting precipitate was collected by filtration, washed three times with methanol, dried and purified by recrystallization from a methanol–water mixture. Elemental analysis (%): Calcd for $Na_3Eu\mathbf{L}Cl_3{\cdot}2H_2O$ (642.58): C, 20.54; H, 1.71; N, 4.36; Found: C, 20.47; H, 1.74; N, 4.31; IR (KBr), ν/cm^{-1}:3430, 3270, 3054, 1590, 1502, 1431, 1404, 1353, 1330, 619, 420; Elemental analysis (%): Calcd for $Na_3Tb\mathbf{L}Cl_3{\cdot}3H_2O$ (667.52): C, 19.77; H, 1.95; N, 4.19; Found: C, 19.82; H, 1.91; N, 4.22; IR (KBr), ν/cm^{-1}: 3407, 1587, 1497, 1401, 1351, 1304, 1256, 621, 421.

Interactions with BSA

Fluorescence spectrum

A 2.5 mL solution containing 1.0×10^{-5} mol L^{-1} BSA was titrated by successive additions of 1.0×10^{-3} mol L^{-1} stock solution of **L**, Eu**L**, Tb**L** and the concentration of it varied from 0 to 1.0×10^{-4} mol L^{-1}. Titrations were done manually by using micro-injector. An excitation wavelength (Ex) of 280 nm was chosen in the experiment. The excitation and emission slit widths (5 nm each) and scan rate (240 nm min^{-1}) were constantly maintained for all experiments. The fluorescence spectra were recorded at 300, 310 and 320 K in the range of 300–440 nm, respectively. The temperatures of the samples were kept by recycled water throughout the experiment.

UV–Vis absorption spectroscopy

Absorption spectra (UV) measurements were recorded at 300 K in the region of 210–320 nm. The 2.5 mL of BSA stock solution was titrated with successive additions of the working solution. The HCl–Tris buffer solution was used as a reference solution.

Results and discussion

Properties of the complexes

Elemental analyses

The results of elemental analyses of C, H, and N are in accordance with the theoretical values calculated, indicating that the composition of the complexes are $Na_3Eu\mathbf{L}Cl_3{\cdot}2H_2O$ and $Na_3Tb\mathbf{L}Cl_3{\cdot}3H_2O$. We suspected that the chemical structure of complexes (Scheme 2) as given below.

FT-IR spectra

The characteristic infrared absorption bands of the free **L** and its Eu(III) and Tb(III) complexes which are useful for suggesting the mode of coordination of ligands are given in Table 1. The FT-IR spectra of the two complexes are similar, indicating that they are structurally alike (Fig. 1). The FT-IR spectrum of the free **L** shows bands at 3078 cm^{-1} attributed to free ν(OH) of –COOH. The bands at 1717 and 1571 cm^{-1} are assigned to ν(C=O) of the carboxyl group and ν(C=N) of **L** respectively. In the complexes, the band for ν(C=N) of the pyridine ring shows a shift to low frequency from 1571 to 1498–1502 cm^{-1} as a result of the coordination through

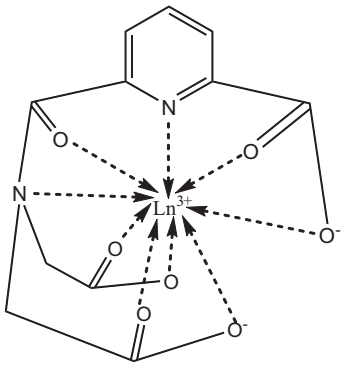

Scheme 2. The chemical structure of the complexes.

Table 1
Characteristic IR bands (cm^{-1}) of the ligand and its complexes.

Sample	ν(OH)	ν(C=O) of carboxyl	ν_{as}(COO−)	ν_s(COO−)	ν_{py}(C=N)
L	3078	1717			1571
$Na_3EuLCl_3{\cdot}2H_2O$	3430		1590	1404	1502
$Na_3TbLCl_3{\cdot}3H_2O$	3407		1587	1401	1498

ν_{as}, asymmetric; ν_s, symmetric.

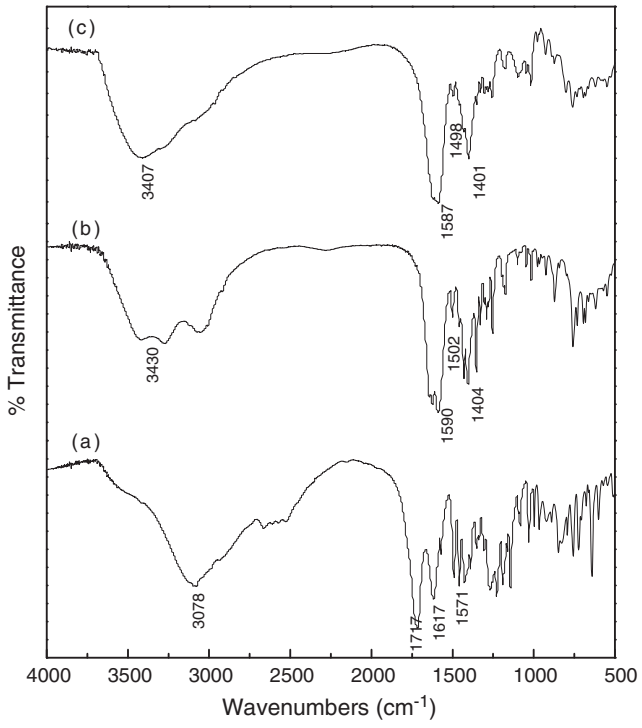

Fig. 1. IR spectrum of **L** (a), Eu(III) complex (b) and Tb(III) complex(c).

metal-nitrogen bond [17]. The band ν(C=O) at 1717 cm^{-1} for free **L** disappeared and new bands appeared at 1580–1590 cm^{-1} and 1401–1404 cm^{-1} which are assigned to the two characteristic bands of asymmetric (ca. 1600 cm^{-1}) and symmetric (ca. 1400 cm^{-1}) stretching vibration modes of the carboxylate group. This indicates that the carboxylic acid group was converted into a carboxylate anion as a result of the formation of the stable Ln(III)-cored complexes [15]. The absorption bands assigned to the ν(Ln–O) and ν(Ln–N) stretching frequencies of the complex are observed at 420 cm^{-1} and 620 cm^{-1} respectively, which also confirmed that the oxygen and nitrogen atoms participated in the coordination [15]. A broad band at 3431–3203 cm^{-1} assigned to ν(OH) indicates the presence of the lattice water which was confirmed in thermal gravimetric analyses (TGA).

TGA

The TGA results of the two complexes $Na_3Eu\mathbf{L}Cl_3{\cdot}2H_2O$ and $Na_3Tb\mathbf{L}Cl_3{\cdot}3H_2O$ are given in Supplementary data (Fig. S1). There are two main successive mass loss stages in the TG curves. For Eu(III) complexes, the first loss in the range of 30–170 °C accounts for the release of the solvated water content (Weight loss: 5.75%, Calcd: 5.60%), the second step occurs in the range of 250–290 °C corresponding to the loss of **L** (Weight loss: 44.62%, Calcd: 43.45%). While for Tb(III) complexes, the first stage of the decomposition appears within 30–180 °C owing to the loss of the solvated water (Weight loss: 7.97%, Calcd: 7.79%). And the second loss stage ranging from 310 to 390 °C is attributed to the loss of **L** (Weight loss: 42.03%, Calcd: 41.83%), which was confirmed by comparing the observed/estimated and the calculated mass of the complexes. The detailed data are listed in Table 2. The above results prove that the water in the complexes was the solvated water and did not participate in coordination, because the coordinated water of the analogous complexes is usually released over 200 °C.

Fluorescence properties of complexes

The emission and excitation spectra measured in the solid state at room temperature are displayed in Figs. 2 and 3, respectively. The luminescence data for the complexes are listed in Table 3. The excitation spectra of the complexes exhibited a broad band between 250 and 400 nm which was attributable to the π–π^* transition of the coordinated ligands. The emission spectra of Eu(III) complexes, obtained with the excitation wavelength of 281 nm, are composed of the typical emission lines for Eu(III) owing to the transitions from the first excited state ($^5D_0$) to the ground multiplet ^7F_J (J = 0–4). The maximum peak intensities at 580, 591, 612, 648, and 694 nm were observed for the J = 0, 1, 2, 3, and 4 transitions, respectively. The transitions of $^5D_0 \rightarrow {}^7F_0$ (forbidden in inversion center) and $^5D_0 \rightarrow {}^7F_3$ (magnetic and electric dipole transitions) are very weak while those of $^5D_0 \rightarrow {}^7F_1$ (magnetic dipole transition) and $^5D_0 \rightarrow {}^7F_2$ are strong. The fact that the hypersensitive $^5D_0 \rightarrow {}^7F_2$ transition is the most intensive indicates a highly polarizable chemical environment around the europium site [18]. The emission spectra of the Tb(III) complexes, obtained with the excitation wavelength of 301 nm, are composed of the typical emission lines for Tb(III), which are assigned to the transitions between the first excited state ($^5D_4$) and the ground multiplet ^7F_J (J = 6–3) (Fig. 3). The emission mechanism of the Tb(III) complex is substantially the same as that of the Eu(III) complex. The emission spectrum of the Tb(III) complex consisted of four main bands at approximate 488 nm ($^5D_4 \rightarrow {}^7F_6$), 544 nm ($^5D_4 \rightarrow {}^7F_5$), 581 nm ($^5D_4 \rightarrow {}^7F_4$) and 618 nm ($^5D_4 \rightarrow {}^7F_3$), and we can see that the emission band at 544 nm is obviously stronger than the other emission bands. In addition, the intensity ratio of the two main bands at 488 nm and 544 nm is about 2.1, which indicates that the Tb(III) ion is at the center of an asymmetric coordination field [19]. Still,

Table 2
TG data of $Na_3Eu\mathbf{L}Cl_3{\cdot}2H_2O$ and $Na_3Tb\mathbf{L}Cl_3{\cdot}3H_2O$.

Complexes	Stage	Temperature range (°C)	Mass loss (%) found (calc.)	Probable lost molecules
$Na_3Eu\mathbf{L}Cl_3{\cdot}2H_2O$	I	30–170	5.75 (5.60)	$2H_2O$
	II	250–290	44.62 (43.45)	**L**
$Na_3Tb\mathbf{L}Cl_3{\cdot}3H_2O$	I	30–180	7.97 (7.79)	$3H_2O$
	II	310–390	42.03 (41.83)	**L**

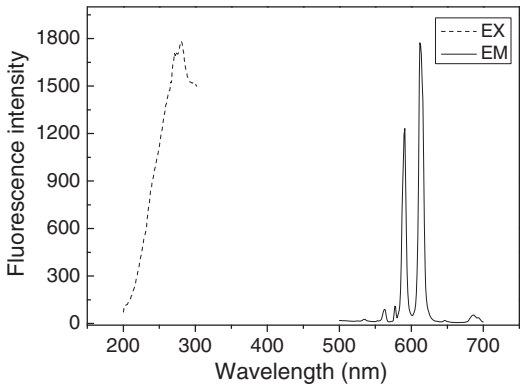

Fig. 2. (Left) Excitation ($^5D_0$–$^7F_2$ transition) and (right) emission (λ_{ex} = 281 nm) spectra of $Na_3EuLCl_3{\cdot}2H_2O$ in the solid state at room temperature.

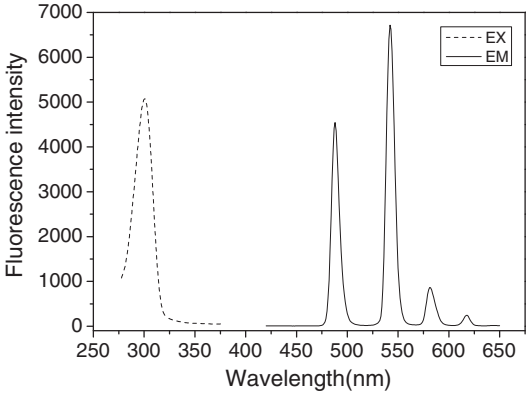

Fig. 3. (Left) Excitation ($^5D_4 \rightarrow {}^7F_5$ transition) and (right) emission (λ_{ex} = 301 nm) spectra of $Na_3TbLCl_3{\cdot}3H_2O$ in the solid state at room temperature.

Table 3
Luminescence data for the complexes.

Complexes	λ_{ex} (nm)	λ_{em} (nm)	LI	Assignment
$Na_3EuLCl_3{\cdot}2H_2O$	281	591	1246	$^5D_0 \rightarrow {}^7F_1$
		612	1773	$^5D_0 \rightarrow {}^7F_2$
$Na_3TbLCl_3{\cdot}3H_2O$	301	488	2387	$^5D_4 \rightarrow {}^7F_6$
		544	6718	$^5D_4 \rightarrow {}^7F_5$
		581	863	$^5D_4 \rightarrow {}^7F_4$
		618	246	$^5D_4 \rightarrow {}^7F_3$

each emission band is very narrow and the widths of half bands are about several nanometers, indicating that the complexes have high color purity [14].

BSA binding studies

*Fluorescence quenching of BSA by **L**, Eu**L** and Tb**L***

The fluorescence quenching mechanisms are usually classified into dynamic quenching and static quenching. For the dynamic quenching mechanism, as the system temperature rises, the effective collision times between molecules, the energy transfer efficiency, and the fluorescence quenching constants of substances will all increase. For the static quenching mechanism, increased temperature reduces the stability of the complex formed, resulting in a reduced quenching constant.

The effect of **L** on the fluorescence emission spectra of BSA at 300 K is shown in Fig. 4, Eu**L** and Tb**L** are shown in Fig. S2, and

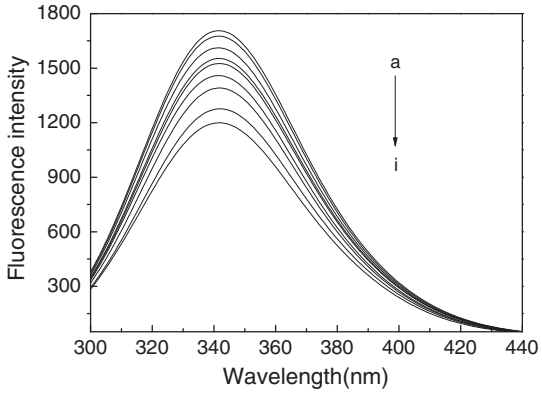

Fig. 4. The quenching effect of **L** on fluorescence intensity of BSA at 300 K; λ_{ex} = 280 nm; $c_{BSA} = 1.0 \times 10^{-5}$ mol L^{-1}; c(**L**)/(10^{-5} mol L^{-1}).(a–i): 0, 0.8, 1.6, 2.4, 3.2, 4, 6, 8 and 10, respectively.

the corresponding calculated results are given in Table 4. The fluorescence intensity of BSA consistently decreased with the addition of **L**, Eu**L** and Tb**L**. At the same time, a slight blue shift at the maximum emission wavelength of BSA was observed, which indicated that there existed strong interaction between **L**, Eu**L** and Tb**L** and BSA, and the microenvironment around the chromophore of BSA was also changed [20]. The quenching can be mathematically expressed by the *Stern–Volmer* Eq. (1), which allows for calculating of quenching constants [21]:

$$\frac{F_0}{F} = 1 + K_{sv}[Q] = 1 + \tau_0 k_q [Q] \quad (1)$$

where, kq, Ksv, τ0 and [Q] are the quenching rate constant of BSA (M−1 s−1), the dynamic Stern–Volmer quenching constant (M−1), the average lifetime of BSA and the concentration of quencher (M), respectively. F0 and F are the fluorescence intensities in the absence and presence of quencher, respectively. In fact, the fluorescence lifetime of biomolecular τ0 is about 10−8 s [22]; the biomolecular quenching constant kq at pH 7.40 can be obtained by the linear Stern–Volmer plots of F0/F against [Q] from Eq. (1) at different temperatures. Representative Stern-Volmer plots for L binding to BSA are shown in Fig. 5, and those for EuL and TbL binding to BSA are in Fig. S3. In general, the maximum collision quenching constant (kq) of various kinds of biomolecules is 2.0 × 1010 L mol−1 S−1 [22]. Obviously, the rate constants (Table 4) of BSA quenched by L, EuL and TbL are greater than 2.0 × 1010 L mol−1 S−1, which suggests that the quenching is initiated by static quenching resulting from the complex formation rather than by dynamic quenching, which is confirmed in the following UV–Vis spectra. While the results also show that the values of the Stern–Volmer quenching constants Ksv and kq increased with the increased temperature. It indicates that the probable quenching mechanism of BSA-(L, EuL and TbL) interactions was initiated by the dynamic collision. In other words, the fluorescence quenching of BSA results from the static quenching, while that dynamic collision could be not negligible [23].

Binding constant and binding sites

The relationship between the fluorescence intensity and the concentration of the quenchers can be described by the following Eq. (2) for static quenching:

$$\log[F/(F_0 - F)] = \log\frac{1}{K_a} + n\log\frac{1}{[Q]} \quad (2)$$

where Ka is the binding constant, and n is the number of binding sites per BSA [15]. Fig. 6 shows the double-logarithm algorithm curve of L-BSA system and Table 5 gives the corresponding calculated results. Similar results were obtained for EuL and TbL

Table 4
Stern–Volmer quenching constants K_{sv} and k_q for binding of BSA with **L**, Eu**L** and Tb**L** at different temperatures.

L or Complex	T (K)	K_{sv} ($\times 10^4$ L mol^{-1})	k_q ($\times 10^{12}$ L mol^{-1} S^{-1})	R^2 [a]
L	300	0.43	0.43	0.99662
	310	0.48	0.48	0.99662
	320	0.50	0.50	0.99653
EuL	300	1.16	1.16	0.98994
	310	1.23	1.23	0.99109
	320	1.26	1.26	0.99553
TbL	300	1.17	1.17	0.98861
	310	1.27	1.27	0.99446
	320	1.35	1.35	0.99882

[a] R^2 is the correlation coefficient of Stern–Volmer equation.

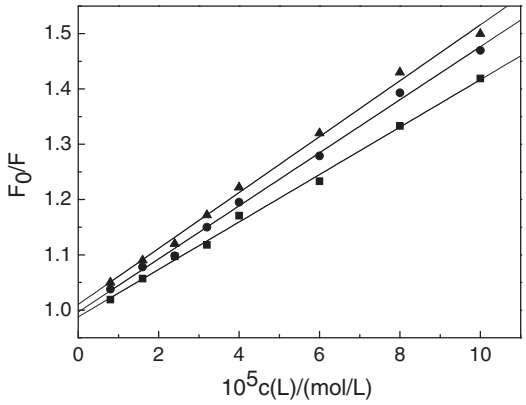

Fig. 5. Stern–Volmer plots of fluorescence quenching of BSA by **L** at three different temperatures (■300 K; ●310 K; ▲320 K).

(Fig. S4). These results suggest that there is a strong binding force between L, EuL and TbL with BSA. According to Table 5, the corresponding binding sites n at the temperatures of 300 K, 310 K and 320 K were roughly equal to 1.0, indicating that the interaction of the complex with BSA has only a single binding site. The binding constants of the interaction between L, EuL and TbL with BSA increase in the following order: TbL > EuL > L at different temperatures, which means that TbL has the strongest ability to bind with BSA, while L is the weakest. The two factors may result in the binding potency of L, EuL and TbL and BSA: (1) Ln(III) ionic radius; (2) the increasing polarity of the complex than that of the ligand strengthening its binding affinity [23,24].

Thermodynamic parameters and binding mode

The interaction forces between proteins and ligands may include hydrophobic, hydrogen bonds, van der Waals, electrostatic interactions, etc. In order to elucidate the interaction between **L**, Eu**L** and Tb**L** with BSA, the thermodynamic parameters were calculated from the *van't Hoff* plots. If the enthalpy change (ΔH) does not vary significantly in the temperature range studied, both the enthalpy change (ΔH) and entropy change (ΔS) can be evaluated from the *van't Hoff* equation [24]:

$$\ln K_a = -\frac{\Delta H}{RT} + \frac{\Delta S}{R} \quad (3)$$

where Ka is analogous to the associative binding constants at the corresponding temperature and R is the gas constant. The calculation was carried out at three different temperatures, which are 300, 310, and 320 K. ΔH is calculated from the slope of the van't Hoff relationship. The free energy change (ΔG) is then estimated from the following relationship:

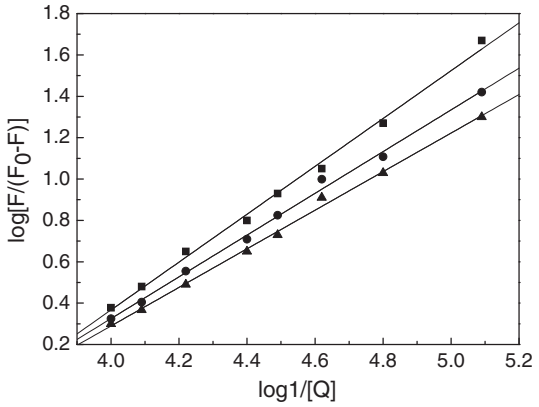

Fig. 6. Double-log plot of **L** quenching effect on BSA fluorescence at three different temperatures (■300 K; ●310 K; ▲320 K).

$$\Delta G = \Delta H - T\Delta S \quad (4)$$

Fig. S5, by plotting the data in Table 5, shows the values of ΔH and ΔS obtained for the binding site from the slopes and ordinates at the origin of the fitted lines. The negative values of ΔG, seen in Table 5, support the assertion that the binding process is spontaneous. When $\Delta H < 0$ or $\Delta H \approx 0$, $\Delta S > 0$, the main acting force is electrostatic force; when $\Delta H < 0$, $\Delta S < 0$, the main acting force is van der Waals or hydrogen bond and when $\Delta H > 0$, $\Delta S > 0$, the main force is hydrophobic [25]. The ΔH and ΔS values of the interactions between **L**, Eu**L** and Tb**L** with BSA indicate that van der Waals interactions and hydrogen bonds play major roles in the binding reaction.

BSA conformation investigation

The synchronous fluorescence spectra can provide much valuable information about the microenvironment in the vicinity of the chromophore molecules [26]. In the synchronous fluorescence of BSA, the shift in the position of the maximum emission wavelength corresponds to the changes of the polarity around the fluorophore of amino acid residues. When $\Delta\lambda$ values are stabilized at 15 or 60 nm, the synchronous fluorescence of BSA is characteristic of tyrosine residues (Tyr) and tryptophan residues (Trp), respectively [27]. The effect of **L** on BSA synchronous fluorescence spectroscopy is shown in Fig. 7. As seen from it, the fluorescence of Tyr was weak and the position of maximum emission wavelength had no change when $\Delta\lambda$ was 15 nm. However, the fluorescence of Trp was strong and the maximum emission wavelength moderately shifted toward short wave when $\Delta\lambda$ was 60 nm. This reflects that the microenvironment of the Trp was significantly affected by **L** binding. The slight blue shift of Trp fluorescence indicates that the polarity around the tryptophan residue decreases and the hydrophobicity increases [28].

UV–Vis absorption measurement is a very simple method and applicable to exploring the structural change and to know the complex formation [29]. To explore the structural change of BSA by the addition of **L**, the UV–Vis spectra of BSA with various amounts of **L** and its Eu(III) and Tb(III) complexes were measured. Fig. 8 shows the UV–Vis absorption spectra of BSA from 210 to 315 nm in the presence of different **L** concentrations. As shown in Fig. 8, **L** has almost non-UV absorption under the present experimental conditions, while BSA has a strong absorbance with a peak at 280 nm. The peak at 280 nm corresponds to the absorption of the $\pi-\pi^*$ transition of amino acid residues (Trp, Tyr) in protein. Upon the addition of **L** to the solution of BSA, it is found that the absorption of BSA increased regularly as the peak shows a blue shift at 280 nm (from 278.0 nm to 271.3 nm). The hyperchromicity and the shift

Table 5
The binding constant (K_a), binding sites (n) and relative thermodynamic parameters for the interactions of **L**, Eu**L** and Tb**L** with BSA at 300 K, 310 K and 320 K, respectively.

L or Complex	T (K)	K_a (L·mol^{-1})	n	R^2 [a]	ΔH (kJ mol^{-1})	ΔS (J mol^{-1} K^{-1})	ΔG (kJ mol^{-1})	R^2 [b]
L	300	2.22×10^4	1.17	0.98154	−84.69	−198.95	−25.01	0.9987
	310	6.91×10^3	1.00	0.99573			−23.02	
	320	2.82×10^3	0.93	0.99653			−21.02	
EuL	300	1.33×10^5	1.27	0.98697	−83.01	−178.09	−29.58	0.99396
	310	4.92×10^4	1.15	0.99749			−27.80	
	320	1.64×10^4	1.03	0.99719			−26.02	
TbL	300	4.27×10^5	1.39	0.99972	−93.01	−202.14	−32.37	0.99095
	310	1.47×10^5	1.27	0.99877			−30.35	
	320	4.07×10^4	1.13	0.99827			−28.33	

[a] R^2 is the correlation coefficient of double-logarithm equation.
[b] R^2 is the correlation coefficient of the value of ΔH, ΔS.

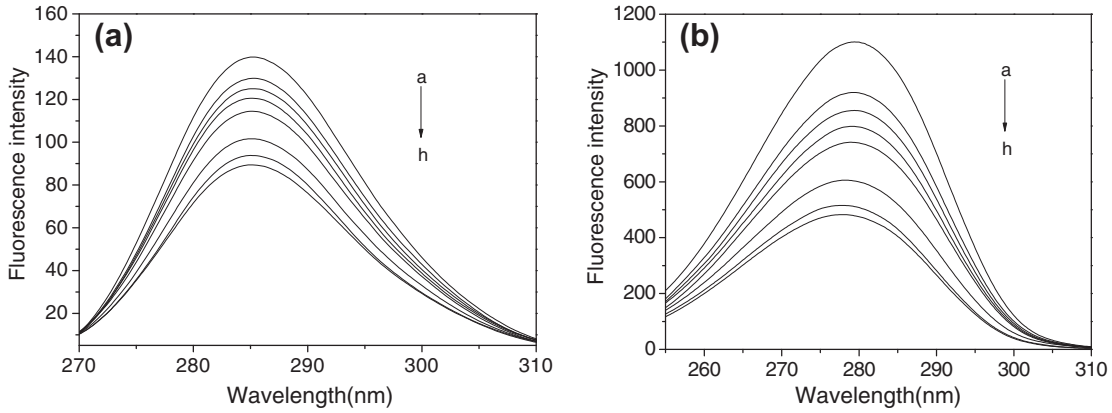

Fig. 7. Effect of **L** on the synchronous fluorescence spectra of BSA. (a) $\Delta\lambda$ = 15 nm, (b) $\Delta\lambda$ = 60 nm; T = 298 K; c(BSA) = 1.0×10^{-5} mol L^{-1}; c(**L**)/(10^{-5} mol L^{-1}), a–h: 0, 0.1, 0.2, 0.3, 0.4, 0.6, 0.8, 1.0, respectively.

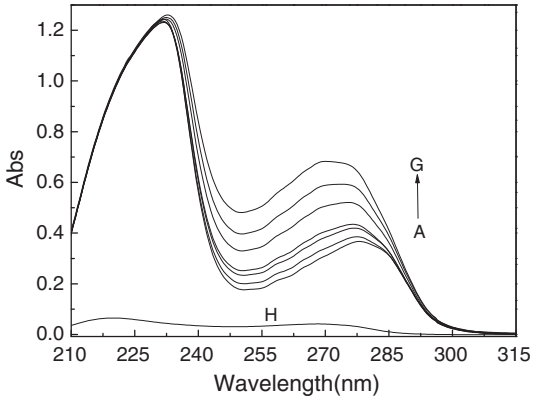

Fig. 8. UV–Vis absorption spectra of BSA in the presence of L at 298 K. Curve H: c(BSA) = 0; c(**L**) = 1.0×10^{-5} mol L^{-1}, Curve A → G: c(BSA) = 1.0×10^{-5} mol L^{-1}, c(**L**)/(10^{-5} mol L^{-1}), (A–G): 0, 1, 2, 3, 5, 7 and 10, respectively.

effect suggest that the conformation of BSA was changed with the addition of **L** [30].

Its Eu(III) and Tb(III) complexes presented a similar synchronous fluorescence and UV–Vis absorption spectra characteristics. The results indicate that the interactions of **L** and its Eu(III) and Tb(III) complexes cause conformational change of BSA.

Conclusions

A novel aromatic carboxylic acid ligand **L** were synthesized and its corresponding complexes with Eu(III) and Tb(III) were successfully prepared. The study of the luminescence properties of the complexes showed that Eu(III) and Tb(III) could be sensitized efficiently by the ligand. The interactions of **L**, Eu**L** and Tb**L** with BSA have been investigated through fluorescence spectroscopy under physiological conditions. The probable quenching mechanism of the fluorescence of BSA by **L** and its Eu(III) and Tb(III) complexes was static quenching. Van der Waals interactions and hydrogen bonds played major roles in the binding reaction. In addition, the binding affinity of them to BSA was determined to be in the order of Tb**L** > Eu**L** > **L**, indicating that the addition of the rare earth ion to the **L** center is helpful to the binding of BSA. The synchronous fluorescence spectra and UV–Vis absorption spectroscopy indicated that the interaction of **L** and its Eu(III) and Tb(III) complexes with BSA caused conformational change of BSA. These results are expected to give important insight into interactions of the rare earth complexes and BSA, which show great reference value for a model of application for drug design.

Acknowledgement

Financial support from the National Natural Science Foundation of China (No. 21071152) is Gratefully acknowledged.

Appendix A. Supplementary data

Supplementary data associated with this article can be found, in the online version, at http://dx.doi.org/10.1016/j.saa.2012.08.060.

References

[1] R. Feng, F.L. Jiang, M.Y. Wu, L. Chen, C.F. Yan, M.C. Hong, Cryst. Growth Des. 10 (2010) 2306–2313.
[2] J. Claude, G. Bünzli, Acc. Chem. Res. 39 (2006) 53–61.

[3] S.V. Eliseeva, J. Claude, G. Bünzli, Chem. Rev. 39 (2010) 189–227.
[4] J.L. Yuan, G.L. Wang, TrAC – Trends Anal. Chem. 25 (2006) 490–500.
[5] J.G.H. du Preez, H.E. Rohwer, B.J. van Brecht, M.R. Caira, J. Chem. Soc. Dalton Trans. 5 (1984) 975–980.
[6] S.S. Krishnmurthy, S. Soundarajan, Z. Anorg, Allg. Chem. 348 (1996) 309–312.
[7] A. Datta, N.K. Karan, S. Mitra, V.J. Gramlich, J. Chem. Crystallogr. 33 (2003) 579–583.
[8] B. Gillon, C. Mathoniere, E. Ruiz, S. Alvarez, A. Cousson, T.M. Kahn, J. Am. Chem. Soc. 124 (2002) 14433–14441.
[9] M. Xu, Z.R. Ma, L. Huang, F.J. Chen, Z.Z. Zeng, Spectrochim. Acta A 78 (2011) 503–511.
[10] C.P. Montgomery, E.J. New, D. Parker, R.D. Peacock, Chem. Commun. 36 (2008) 4261–4263.
[11] G. Zolese, G. Falcioni, E. Bertoli, R. Galeazzi, M. Wozniak, Z. Wypych, E. Gratton, A. Ambrosini, Proteins 40 (2000) 39–48.
[12] D.C. Carter, J.X. Ho, Adv. Protein Chem. 45 (1994) 153–203.
[13] A. Brockhinke, R. Plessow, K. Kohse-Hoinghaus, C. Herrmann, Phys. Chem. Chem. Phys. 5 (2003) 3498–3506.
[14] R.R. Tang, C.H. Tang, C.Q. Tang, J. Organomet. Chem. 696 (2011) 2040–2046.
[15] W. Brzyska, W. Ozga, Thermochim. Acta 247 (1994) 329–339.
[16] C. Schmuck, U. Machon, Chem. Eur. J. 11 (2005) 1109–1118.
[17] K.R. Surati, Spectrochim. Acta A 79 (2011) 272–277.
[18] T.Y. Zhu, K. Ikarashi, T. Ishigaki, K. Uematsu, K. Toda, H. Okawa, M. Sato, Inorg. Chim. Acta 362 (2009) 3407–3414.
[19] G.F. de Śa, O.L. Malta, C. de Mello Doneǵa, A.M. Simas, R.L. Longo, P.A. Santa-Cruz, E.F. da Silva Jr., Coord. Chem. Rev. 196 (2000) 165–195.
[20] T.H. Wang, Z.M. Zhao, L. Zhang, L. Ji, J. Mol. Struct. 937 (2009) 65–69.
[21] Y.C. Liu, Z.Y. Yang, J. Organomet. Chem. 694 (2009) 3091–3101.
[22] J.R. Lakowicz, G. Weber, Biochemistry 12 (1973) 4161–4170.
[23] X.Y. Yu, Y. Yang, S.Y. Lu, Q. Yao, H.T. Liu, X.F. Li, P.G. Yi, Spectrochim. Acta A 83 (2011) 322–328.
[24] Y.J. Hu, O.Y. Yu, A.M. Bai, R.M. Zhao, Y. Liu, Biol. Trace Elem. Res. 136 (2010) 8–17.
[25] Y.T. Sun, H.T. Zhang, Y. Sun, Y.P. Zhang, H. Liu, J.H. Cheng, S.Y. Bi, H.Q. Zhang, J. Lumin. 130 (2010) 270–279.
[26] B. Klajnert, M. Bryszewska, Bioelectrochemistry 55 (2002) 33–35.
[27] H. Yan, S.L. Zhao, J.G. Yang, X.D. Zhu, G.L. Dai, H.D. Liang, F.Y. Pan, L. Weng, J. Solution Chem. 38 (2009) 1183–1192.
[28] X.L. Shi, X.W. Li, M.Y. Gui, H.Y. Zhou, R.J. Yang, H.Q. Zhang, Y.R. Jin, J. Lumin. 130 (2010) 637–644.
[29] Z.J. Cheng, Y.T. Zhang, J. Mol. Struct. 879 (2008) 81–87.
[30] X.L. Liu, J.J. Fan, Y. Liu, A.X. Hou, J. Mol. Struct. 934 (2009) 1–8.